Environmental Science & Technology

Article

pubs.acs.org/est

Influence of Dissolved Silicate on Rates of Fe(II) Oxidation

Andrew S. Kinsela,[†,‡] Adele M. Jones,[†] Mark W. Bligh,[†,‡] An Ninh Pham,[†] Richard N. Collins,[†] Jennifer J. Harrison,[‡] Kerry L. Wilsher,[‡] Timothy E. Payne,[‡] and T. David Waite*[,†]

[†]School of Civil and Environmental Engineering, The University of New South Wales, Sydney, New South Wales 2052, Australia

[‡]Institute for Environmental Research, Australian Nuclear Science and Technology Organisation, Locked Bag 2001, Kirrawee DC, New South Wales 2232, Australia

Supporting Information

ABSTRACT: Increasing concentrations of dissolved silicate progressively retard Fe(II) oxidation kinetics in the circum-neutral pH range 6.0−7.0. As Si:Fe molar ratios increase from 0 to 2, the primary Fe(III) oxidation product transitions from lepidocrocite to a ferrihydrite/silica-ferrihydrite composite. Empirical results, supported by chemical kinetic modeling, indicated that the decreased heterogeneous oxidation rate was not due to differences in absolute Fe(II) sorption between the two solids types or competition for adsorption sites in the presence of silicate. Rather, competitive desorption experiments suggest Fe(II) was associated with more weakly bound, outer-sphere complexes on silica-ferrihydrite compared to lepidocrocite. A reduction in extent of inner-sphere Fe(II) complexation on silica-ferrihydrite confers a decreased ability for Fe(II) to undergo surface-induced hydrolysis via electronic configuration alterations, thereby inhibiting the heterogeneous Fe(II) oxidation mechanism. Water samples from a legacy radioactive waste site (Little Forest, Australia) were shown to exhibit a similar pattern of Fe(II) oxidation retardation derived from elevated silicate concentrations. These findings have important implications for contaminant migration at this site as well as a variety of other groundwater/high silicate containing natural and engineered sites that might undergo iron redox fluctuations.

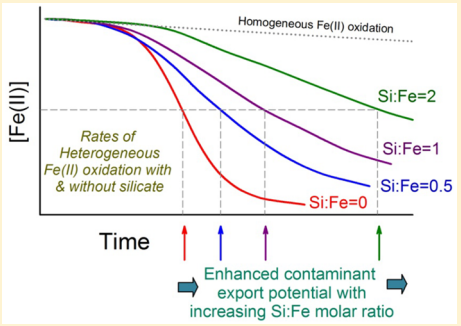

INTRODUCTION

The oxidation of soluble Fe(II) and resultant precipitation of Fe(III) oxyhydroxides in transitioning from reduced to oxic environments is a key process determining the fate of contaminants at sites exhibiting such redox variability.[1] This is due to the inherent physicochemical properties of freshly formed Fe(III) oxyhydroxides, which have the capacity to adsorb and/or incorporate a variety of organic and inorganic contaminants, including radionuclides. As Fe(III) oxyhydroxides, henceforth referred to as Fe(III) oxides, confer a vastly different transport behavior upon any associated contaminants when compared to their dissolved counterparts, the mobility of these contaminants is therefore strongly influenced by Fe(II) oxidation kinetics.

At low (nanomolar to low micromolar) Fe(II) concentrations, the rate of oxidation by molecular oxygen has been shown to be reasonably described by the homogeneous rate expression shown in eq 1[2] with the rate constant, k, strongly dependent on the dissolved Fe(II) speciation.[3,4]

$$-\mathrm{d[Fe(II)]}/\mathrm{d}t = k[\mathrm{OH^-}]^2 P_{O2}[\mathrm{Fe(II)}] \quad (1)$$

However, at higher concentrations of dissolved Fe(II), the Fe(III) oxides which form have been shown to catalyze the oxidation process with the extent of surface catalysis becoming more significant with ongoing Fe(III) solid production.[5,6] This heterogeneous oxidation of Fe(II), when undertaken at a constant pH and O_2 concentration, and in the presence of a large amount of Fe(III) oxide, may be described empirically by eq 2, where k and k' are the rate constants for the homogeneous and heterogeneous reactions, respectively.[6]

$$-\mathrm{d[Fe(II)]}/\mathrm{d}t = -(k + k'[\mathrm{Fe(III)}])[\mathrm{Fe(II)}] \quad (2)$$

While k can be derived through integration of eq 1, the heterogeneous rate constant (k') is defined by eq 3.

$$k' = k_s K/[\mathrm{H^+}] \quad (3)$$

The terms k_s and K are, respectively, the reaction rate constants for the oxidation of adsorbed Fe(II) (by oxygen) and the stability constant of Fe(II) adsorption onto a solid Fe(III) oxide (which is strongly affected by pH).[6] Consequently, the adsorption of Fe(II) onto the Fe(III) oxide, at a specific pH, is integral to the autocatalytic oxidation process. Indeed, the results of experiments within the pH range 4.5−5.5 showed that overall rates of Fe(II) oxidation were proportional to the concentration of adsorbed Fe(II).[5] Variations in the rate constant for oxidation of adsorbed Fe(II) (k_s) and the equilibrium adsorption constant (K) have also been shown to account for differences in heterogeneous rate constants (k') between the Fe(III) oxides ferrihydrite and lepidocrocite.[7]

Received: June 16, 2016
Revised: September 8, 2016
Accepted: October 5, 2016
Published: October 5, 2016

DOI: 10.1021/acs.est.6b03015
Environ. Sci. Technol. 2016, 50, 11663−11671

While the rate expressions presented above provide a reasonable description of the effect of oxygen concentration and pH on Fe(II) oxidation rates in solutions of simple compositions, the rates are further altered by the presence of organic[8,9] and inorganic co-ions present in solution.[10−12] Of particular relevance to this research is the influence of dissolved silicate, a ubiquitous component of soils and groundwaters, on the rate of Fe(II) oxidation. The findings of previous research are varied with the presence of silicate shown to increase[10,12] or decrease[11] the rate of homogeneous Fe(II) oxidation. The work of Wolthoorn et al.[12] has provided the only evidence that silicate (0.5 Si:Fe molar ratio) can retard the heterogeneous oxidation of Fe(II) but to a lesser degree than phosphate, manganese and fulvic acid.

It is well-known that the presence of silicate during Fe(II) oxidation strongly alters the Fe(III) hydrolysis and precipitation processes, with the formation of the end-product ferrihydrite, favored over lepidocrocite at circum-neutral pH.[13−15] Indeed, a large body of research has been devoted to understanding the structural implications of varied Si:Fe ratios on the solid-phases formed as well as their differing contaminant retention properties.[16−21] At Si:Fe molar ratios <0.1 to 0.2, poorly ordered lepidocrocite will form. At higher molar ratios, the silicate oxyanion will bind to the corner-sharing Fe surface sites, resulting in the preferential precipitation of silica-ferrihydrite.[21−23]

Although previous research has shown that dissolved silicate induces change to surface charge and stability of colloidal Fe(III) oxides,[17] there is little clarity regarding the effect of silicate concentration on the rate of Fe(II) oxidation or, if there is an effect, on the implications to contaminant transport. This is surprising considering the relevance to a range of naturally occurring and engineered environments that typically exhibit high Fe(II) concentrations including acid sulfate soils containing trace metals,[24] Fe(II)-dosed treatment of contaminated anoxic groundwaters,[25] mine drainage affected areas[26] and shallow groundwaters containing radionuclides.[27] The latter scenario is of interest here, with particular attention given to the effects of silicate concentrations on rates of Fe(II) oxidation and the implications for low-level radioactive waste (LLRW) contained within disposal trenches at a legacy waste site in Australia.

The disposal of LLRW in shallow trenches was a commonly accepted practice in the mid to latter part of the 20th century, and this has resulted in the existence of numerous legacy sites across the globe.[28] Such disposal techniques have since been shown to be generally inadequate for the retention of radionuclides such as Pu.[29−31] Although some sites, such as Maxey Flats in the United States and Harwell in the United Kingdom, have undergone remediation, many legacy trench sites remain, including the Little Forest legacy low-level waste site, on the outskirts of the city of Sydney, Australia. The results of previous studies suggest that the major mechanism by which the LLRW (especially Pu and Am) is dispersed from the trenches is by a "bathtub" effect, whereby the former trenches, located in relatively impermeable clay layers, rapidly fill with water during intense rainfall events and subsequently overflow to the surrounding topsoil.[28] A key topic of interest is therefore the evolution of trench water chemistry during and subsequent to rainfall events. Analyses of these trench waters have revealed elevated concentrations (>1 mM) of dissolved ferrous iron with adsorption of Pu and Am to the Fe(III) oxides that are formed on oxidation of this Fe(II) (particularly following the influx of oxic rainwater) likely one of the most important factors accounting for their retention within the vicinity of the trenches.

The primary objectives of this research were (i) to systematically examine the rates of Fe(II) oxidation in both environmental and synthetic analogue samples under conditions relevant to those at the Little Forest site, and (ii) to assess the role that dissolved silicate plays in changing reaction kinetics. The results of these studies have provided significant insights into the manner in which silicate influences both the rate of Fe(II) oxidation and the nature of the solid Fe(III) oxides formed.

MATERIALS AND METHODS

Sample Collection. Trench water samples were obtained from the Little Forest Legacy Site via a sampling point which derives water from within one of the former trenches.[28] As described in more detail elsewhere,[28,32,33] LLRW was buried in shallow trenches at this site between 1960 and 1968, with subsequent evidence of limited Pu and Am mobilization away from the initial disposal location. Samples were collected via a screened borehole[27,28] using a low-flow centrifugal pump and maintained at 4 °C until commencing analyses soon after. The major inorganic components are listed in the Supporting Information (SI), Table S1. Samples contained both Fe(II) and silicate in a Si:Fe molar ratio of 0.55. The LLRW at Little Forest was disposed of in steel drums[34] along with other metallic items which, together with the highly weathered shale of the local geology,[32] most likely contribute to high dissolved iron concentrations.

Reference Fe(III) oxides lepidocrocite, ferrihydrite (2-line) and silica-ferrihydrite were synthesized according to the procedures outlined by Cornell and Schwertmann[35] and Jones et al.,[13] with only minor modifications. The precipitation of silica-ferrihydrite via this method in which equimolar quantities of Fe(III) and Si are added results in the incorporation of Si into the ferrihydrite structure[13] giving a final concentration of 7.1 wt % Si. Further details are provided in the Supporting Information.

Fe(II) Oxidation. In order to simulate the interaction of oxic rainwater mixing with reduced trench waters rich in Fe(II), all oxidation experiments were undertaken at initial Fe(II) concentrations approximately equating to a 10- and 50-fold dilution of this natural system, that is, 5 mg L^{-1} (0.0895 mM) and 1 mg L^{-1} (0.0179 mM) Fe(II). In addition, simplified synthetic analogues representing trench waters were prepared and analyzed, in order to investigate the effect of dissolved silicate on Fe(II) oxidation kinetics.

Synthetic Solutions. Reaction flasks initially contained an aerated buffer matrix consisting of 1 mM NaCl and 15 mM of noncomplexing, organic buffers[36] MOPS (3-(N-morpholino)-propanesulfonic acid) or MES (2-(N-morpholino)-ethanesulfonic acid). Varying concentrations of silicate (10 mM Si stock solution, pH unadjusted) were added, to achieve Si:Fe molar ratios of 0 (silicate absent), 0.5, 1, and 2. The pH was set to 6.0, 6.5, or 7.0 (±0.05) using NaOH and HCl. The oxidation reaction was initiated by adding an aliquot of $FeCl_2.4H_2O$ (in 10 mM HCl) to achieve a Fe(II) concentration of exactly 0.0895 mM or 0.0179 mM.

Trench Water. As the intention was to investigate the effect of oxic rainfall dilution on rates of Fe(II) oxidation, the trench waters were similarly diluted to achieve initial concentrations of 0.0895 mM or 0.0179 mM Fe(II). Therefore, the same buffer

DOI: 10.1021/acs.est.6b03015
Environ. Sci. Technol. 2016, 50, 11663−11671

matrix described above was prepared and the pH adjusted to 6.0, 6.5, or 7.0. No addition of silicate was made, and thus the Si:Fe molar ratio was set by their intrinsic values (Si:Fe = 0.55, Table S1). The reaction was then initiated by adding known aliquots of the trench water (containing 1.02 mM Fe(II)) to achieve concentrations of 0.0895 mM or 0.0179 mM.

The Fe(II) oxidation kinetics were followed by measuring the loss of Fe(II) from solution via absorbance measurements of the Fe(II)-phenanthroline complex.[37] Unfiltered samples were analyzed, with concentrations therefore reflecting the sum of both dissolved- and phenanthroline-reactive adsorbed-Fe(II). The effect of particle scattering on absorbance was negligible in the presence of the strongly absorbing Fe(II)-phenanthroline complex. Sample absorbance was measured within minutes of phenanthroline addition, and no reduction of Fe(III) was observed. The pH was measured after Fe(II) oxidation was complete, with minimal drift (±0.05) recorded.

Numerous mixing/aeration techniques were examined to assess whether oxygen saturation was maintained. A magnetic stirring unit (with cross-bar stirrer) operating under high rotation provided consistently fast rates of Fe(II) oxidation, ensuring oxygen concentrations were at or near saturation levels.

Fe(II) Sorption. Fe(II) adsorption to the major expected end-products of Fe(II) oxidation (lepidocrocite and silica-ferrihydrite) was determined by measuring changes in the dissolved Fe(II) concentration on contact with these Fe(III) minerals under anoxic conditions. All experiments were performed in an anaerobic chamber (Coy Laboratory Products) in which a N_2:H_2 gas mix (95:5%) was passed over a palladium catalyst (O_2 < 5 ppm). All solutions were purged of O_2 by sparging with high-purity argon gas for >1.5 h.

The amounts of lepidocrocite and silica-ferrihydrite used for the sorption experiments were normalized for Fe(III) content, which was determined by acidic dissolution and quantified by ICP-OES. Dissolved Fe(II), either as stock solutions of $FeCl_2.4H_2O$ or $(NH_4)_2Fe(SO_4).6H_2O$ were added to Fe(III) oxide suspensions, in molar ratios of 1:10 and 1:20, and buffered with 50 mM MES or MOPS. Competitive sorption effects were examined by adding dissolved silicate in Si:Fe molar ratios of 1 and 2 with the silicate introduced simultaneously with aqueous Fe(II). Samples were mixed on an orbital shaker for 10 min with the sorption time intentionally kept short in order to minimize possible Fe(II)-catalyzed transformation of the Fe(III) minerals.[13] After 10 min, a well-mixed aliquot was centrifuged and the resulting supernatant added to a phenanthroline solution in order to determine the 'nonsorbed Fe(II)' fraction. An equal volume of ~3.2 mM HCl solution (pH 2.5) was then added to the centrifuged solid-phase. After rapidly mixing and centrifuging, an aliquot was added to a second phenanthroline solution to determine the 'sorbed Fe(II)' concentration. The sum of the nonsorbed and sorbed Fe(II) fractions accorded within 10% of the total amount of Fe(II) added to each suspension, or were discarded.

A mild extraction technique, based on the method of Cismasu et al.[38] was used to investigate the comparative stability of Fe(II) complexes on lepidocrocite and silica-ferrihydrite. Immediately after the 10 min Fe(II) adsorption procedure described above, the suspension was centrifuged and supernatant decanted. An equal volume of 100 mM $CaCl_2$ (pH 6.5) was added to the wet solid and allowed to equilibrate under gentle mixing for 1 h. Following equilibration, the samples were filtered (0.22 μm) and Fe concentrations analyzed by ICP-MS.

Solid-Phase Characterization. After Fe(II) oxidation was complete, samples were analyzed immediately (<1 h) by Fourier Transform Infrared Spectroscopy (FTIR), with the solid-phases (initially separated by centrifugation) subject to a mildly acidic wash (pH 4.0) in order to remove any adsorbed Fe(II) remaining after the oxidation experiment. The acidic wash was followed by further centrifugation and washing in neutral pH, high-purity (milli-Q) water, repeated four times, before resuspending in ~500 μL of milli-Q water. A 5 μL aliquot of this suspension was rapidly dried with high-purity nitrogen gas on a 3-bounce diamond Zn−Se crystal mounted on a FTIR spectrometer with a universal ATR accessory (Frontier TGS detector; PerkinElmer). The same process was followed for analysis of the synthetic Fe(III) oxides, which were analyzed immediately (<1 h) after their formation.

Freeze-dried solid sample pellets from selected Fe(II) oxidation studies were analyzed by Fe *K*-edge (~7112 eV) extended X-ray adsorption spectroscopy (EXAFS) on the XAS beamline at the Australian Synchrotron (Melbourne, Australia). Specific details of the beamline setup are provided in the SI. The proportion and identity of Fe(III) oxide reaction products were determined via direct fitting of k^3-weighted data by least-squares optimization of the linear combination fit (LCF) of the pure reference materials over the *k*-range 2−10 $Å^{-1}$ using the Athena software package.[39]

Kinetic Modeling. The chemical modeling programs KinTek Explorer Pro v5.2[40] and Kintecus v5.20[41] were used to model the collected experimental data and perform sensitivity analyses on the model output. Further details are given in the Supporting Information.

RESULTS AND DISCUSSION

Heterogeneous Fe(II) Oxidation Kinetics: Empirical Measurements. The decrease in Fe(II) concentrations over time (at pHs 6.0, 6.5 and 7.0) for samples initially containing 0.0895 M Fe(II) are shown in Figure 1, both for the synthetic analogues (in the presence and absence of dissolved silicate) and for the trench water samples. Equivalent results for waters containing 0.0179 mM Fe(II) are provided in SI Figure S1. Considering first the synthetic solutions in the absence of any dissolved silicate, the Fe(II) removal rate was initially described by the homogeneous rate expression shown in eq 1 (dashed gray lines in Figure 1 and SI Figure S1) with rate constants consistent with those determined for oxidation of nanomolar concentrations of Fe(II) in the absence of any solid-phase.[3,4] Once Fe(III) oxides formed, the oxidation rate accelerated markedly, presumably from the more rapid rate of oxidation of adsorbed Fe(II). The oxidation rate increased as more Fe(III) oxide solids were formed and new sites became available for Fe(II) adsorption. During later stages of oxidation, when sufficient solid phase had formed, the rate was not limited by the access to sorption sites and declined as Fe(II) in the system was consumed. Although this mechanism describes the overall trends in all data sets, clear decreases in oxidation rates were observed in response to added silicate (Si:Fe ratios 0.5, 1, and 2) (see Figure 1).

For each pH condition, Fe(II) oxidation rates in the trench water were between those of the analogues containing Si:Fe molar ratios of 0.5 and 2. As indicated in the SI (Table S1), the trench water at the time of sampling had a Si:Fe molar ratio of 0.55. If the rates of Fe(II) oxidation were dictated solely by

DOI: 10.1021/acs.est.6b03015
Environ. Sci. Technol. 2016, 50, 11663−11671

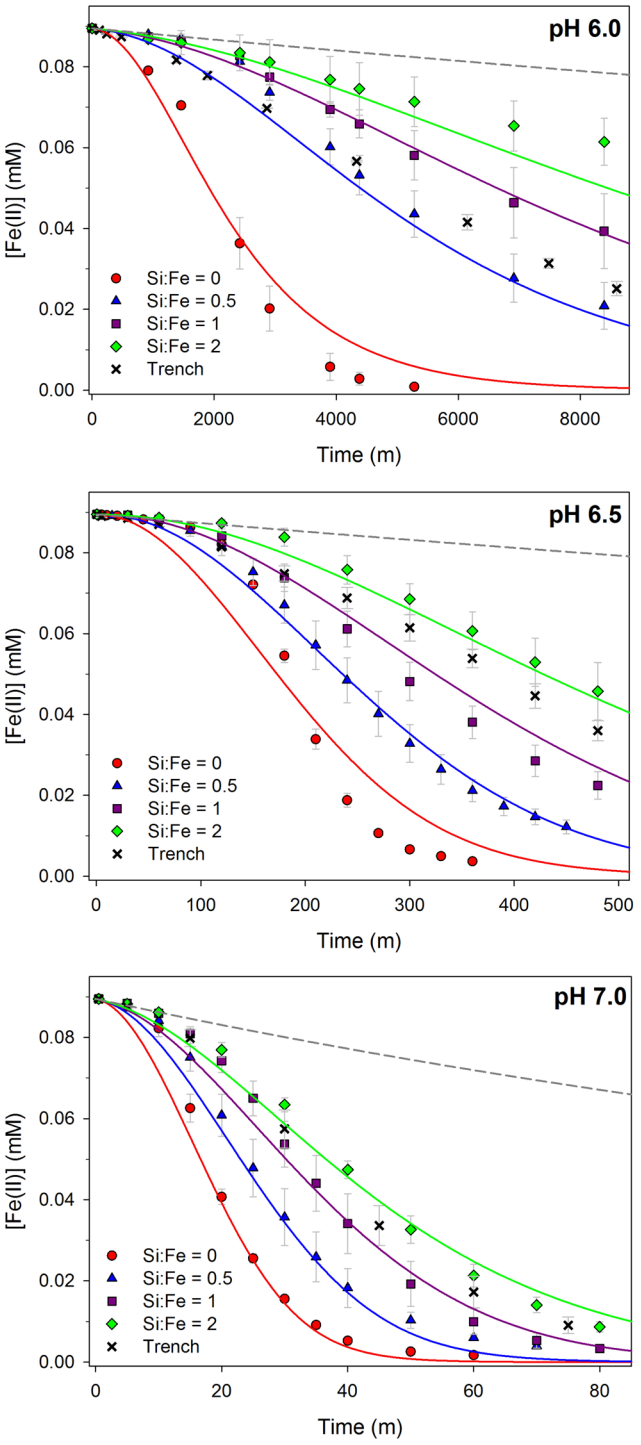

Figure 1. Oxidation of 0.0895 mM Fe(II) from trench and synthetic solutions at pH 6.0 (top), 6.5 (middle) and 7.0 (bottom) in the absence and presence of dissolved silica (data points). Error bars are standard deviations of triplicates. Model outputs (from the reaction scheme in Table 2) are represented by the solid lines. Dashed gray lines represent published homogeneous Fe(II) oxidation rates (refer to Table 2). Note the differing time scales.

interactions with unpolymerized silicate, we would expect the rate to approximately follow the Si:Fe molar ratio of 0.5, which was the case at pH 6 (Figure 1). As pH increased, the Fe(II) oxidation rate of the trench water decreased to rates comparable to Si:Fe molar ratios of between 1 and 2. Understanding the divergence in Fe(II) oxidation kinetics between synthetic analogues and trench waters is difficult due to the inherent differences between single (synthetic) and complex multicomponent (trench) systems with the variability in measurements possibly attributable to several competing factors. Silicate polymerization within trench samples is one factor potentially accounting for the observed variations with pH. Enhanced Si polymerization is more likely either at lower pH or at increased reaction times (e.g., for the pH 6.0 sample set) and would likely lessen the effects of Fe(II) oxidation rate retardation, as observed in Figure 1. However, consideration should also be given to the effects of phosphate, carbonate and organic carbon. Although these components may influence oxidation kinetics through changes to Fe(II) speciation, this is only likely to be minor with the combined proportion and larger rate constants for Fe^{2+}, $Fe(OH)^{+}$ and $Fe(OH)_2$ species[3,4,42] dominating (>99.95%) the overall Fe(II) oxidation rate (SI Figure S2). We suggest a more important divergence from synthetic analogues can be attributed to the impact of additional inorganic and organic ligands inhibiting Fe(III) polymerization and altering Fe(III) oxide mineral structure (discussed below).

Fe(II) Oxidation Product Characterization. Results of FTIR analysis of solids formed from Fe(II) oxidation studies in the absence and presence of dissolved silicate (at pH 7.0) together with FTIR spectra for reference Fe(III) oxides are shown in Figure 2. In the absence of dissolved silicate the FTIR spectra displayed vibration bands characteristic to lepidocrocite

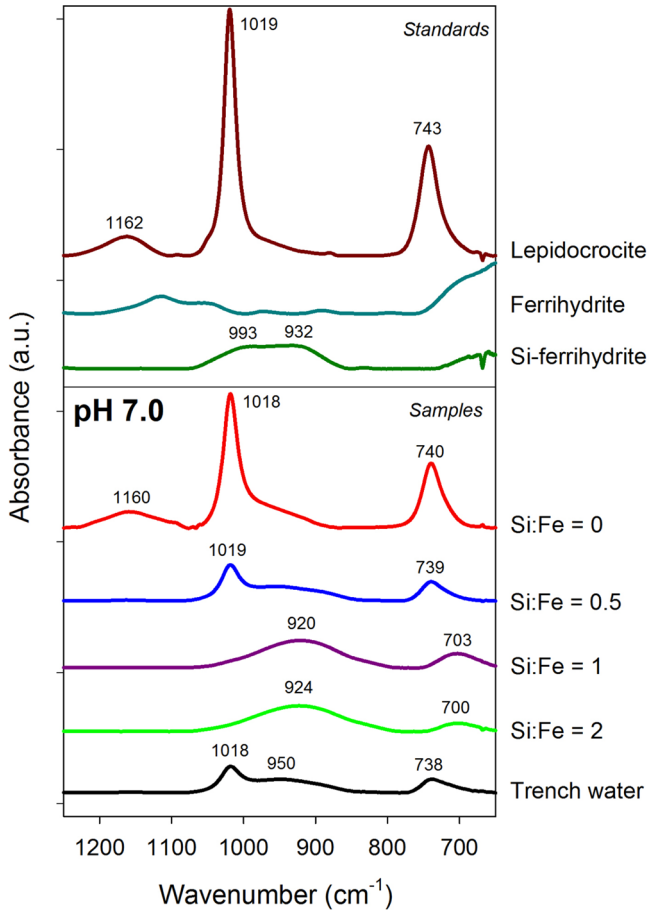

Figure 2. FTIR spectra for Fe(II) oxidation solid-phase products derived from trench and synthetic waters in the absence and presence of silica at varying molar ratios, at pH 7.0.

DOI: 10.1021/acs.est.6b03015
Environ. Sci. Technol. 2016, 50, 11663−11671

(Figure 2). At pH 7.0, in-plane and out-of-plane −OH bending at 1018 and 740 cm^{-1} were evident, consistent with the data generated by Lewis and Farmer[43] for lepidocrocite. Similar bands were observed (±3 cm^{-1}) in the pH 6.5 and 6.0 data (SI Figure S3). The lower peak intensity in the samples compared to the lepidocrocite standard was likely due to the elevated concentrations used to synthesize the lepidocrocite material, which would translate to smaller particles and higher intensity due to greater contact with the FTIR crystal. It is also possible that a higher degree of crystallinity of the lepidocrocite standard compared to the samples might contribute to this effect. As the Si:Fe molar ratio increased, transition to a silica-ferrihydrite-like spectra was observed (Figure 2; SI Figure S3), in accord with previous observations.[15] This was characterized by the progressive weakening in δ−OH and γ−OH bending bands, and commensurate strengthening in a broad vibrational band at 920−950 cm^{-1}, previously attributed to unpolymerized Si stretching from Si−O−Fe bonds (and not Si−O−Si).[15,44] As the Si:Fe molar ratio increased, the major υ(Si−O) vibration band at ∼925 cm^{-1} became a dominant feature. There was no evidence of full Si-polymerization, which would be evident in a Si−O−Si stretching band at 1080 cm^{-1}. However, υ(Si−O) peak broadening was apparent (particularly toward higher wavelengths) for samples prepared in the lower pH treatments (SI Figure S3) where the iron oxide assemblages took longer to form. As observed by Swedlund et al.[45] this shift may indicate the conversion of sorbed Si monomers to an oligomeric phase. Our repeated washing procedure prior to FTIR (and XAS) analysis may well have removed evidence of an oligomeric Si IR signature which may have influenced the Fe(II) oxidation rate measurements.

The trench water samples yielded IR signals similar to that of the 0.5 Si:Fe synthetic samples, with lepidocrocite δ−OH and γ−OH bending remaining visible in the spectrum at all pH (Figure 2, SI Figure S3). A slight shift in the band attributed to Si−O−Fe (from ∼925 cm^{-1} to 949−950 cm^{-1}) likely indicates an increasing degree of partial Si-polymerization in the trench water sample, as suggested to be occurring in the lower pH synthetic samples. This may be associated with a minor aging effect of the natural trench water samples (due to collection/storage and the natural pH being ∼6.6) compared to freshly prepared synthetic analogues. This shift to higher wavelengths associated with aged natural samples is in accordance with findings of Carlson and Schwertmann[44] and their measurements from naturally occurring Si-containing ferrihydrite.

The Fe EXAFS spectra (SI Figure S4) and linear combination fitting (LCF) (Table 1) results were partly consistent with the FTIR data, showing the transition in Fe(III) oxide; from lepidocrocite forming when silica was absent to a ferrihydrite-like structure when Si:Fe > 0.5. Importantly though, the XAS technique can distinguish between ferrihydrite and silica-ferrihydrite structures as a result of the absence of Fe−Fe corner linkages in the latter with this absence reflected by the disappearance of the features at ∼5.5 and 7.5 $Å^{-1}$ (Figure S4) in accord with previous findings.[21] At pH 7.0 and 6.5, the presence of Si at molar ratios up to Si:Fe = 2 did not appear to exclude the formation of ferrihydrite in favor of silica-ferrihydrite though, as noted above, this may be an artifact of our solids rinsing procedure, post formation. At Si:Fe = 2 the relative amounts of ferrihydrite and silica-ferrihydrite were not reliably quantifiable given the less than ideal Fe EXAFS signal.

Table 1. Linear Combination Fitting for Fe(II) Oxidation Solid-Phase Products in the Absence and Presence of Silicate at Varying Molar Ratios, at pH 6.5 and 7.0[a]

pH 6.5	fraction			error
Si:Fe ratio	lepidocrocite	ferrihydrite	silica-ferrihydrite	reduced chi-square
0	0.747	0.253	0.000	0.439
0.5	0.435	0.520	0.045	0.092
1	0.176	0.723	0.101	0.417
2	0.117	0.431	0.452	3.400
pH 7.0	**fraction**			**error**
Si:Fe ratio	lepidocrocite	ferrihydrite	silica-ferrihydrite	reduced chi-square
0	0.855	0.112	0.033	0.162
0.5	0.547	0.379	0.074	0.164
1	0.046	0.721	0.233	0.152
2	0.100	0.615	0.285	4.914

[a]Values were calculated over the k^3-range 2-10 $Å^{-1}$.

Collectively, our observations are in agreement with the large body of research showing that addition of dissolved silicate results in the formation of ferrihydrite at the expense of lepidocrocite.[15,17,18,21,46] This has previously been shown to be a consequence of silicate inhibiting polymerization of Fe(III) and inhibiting corner-sharing Fe linkages, resulting in the formation of smaller-sized, poorly crystalline oxides.[14,16,21]

Fe(II) Sorption to Lepidocrocite and Silica-Ferrihydrite. Since the rate of heterogeneous Fe(II) oxidation is dependent on the extent of sorption and the rate of oxidation of any sorbed Fe(II) species, the Fe(II) sorption capacity for the individual reference materials lepidocrocite and silica-ferrihydrite was investigated (Figure 3). At 1:10 Fe(II):Fe(III) ratio, the percentage of Fe(II) sorbed to both iron oxides increased from <10% at pH 6, to 30−40% at pH 7, characteristic of the Fe(II) adsorption edge on Fe(III) oxides. A similar, albeit more linear, trend was observed at the higher Fe(II):Fe(III) (1:1) ratio (SI Figure S5).

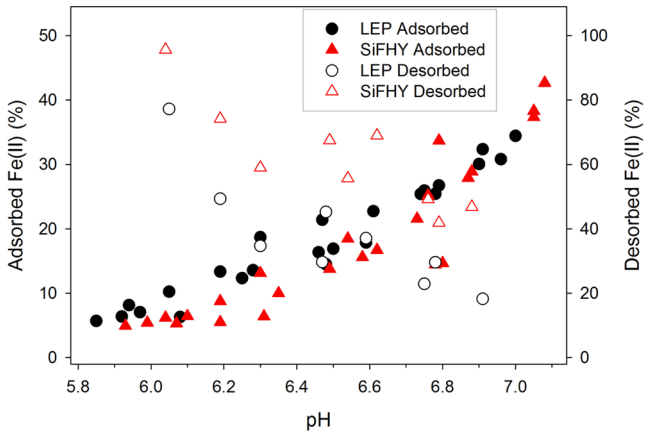

Figure 3. Adsorption of Fe(II) to lepidocrocite (LEP) and silica-ferrihydrite (SiFHY) as a function of pH and normalized to Fe(III) content at molar ratios of 1:10 Fe(II):Fe(III) (solid symbols, left *y*-axis); and percentage Fe(II) desorbed from LEP and SiFHY after $CaCl_2$ extraction (open symbols, right *y*-axis).

Only a minor difference in the Fe(II) sorption capacity between the two reference solids was evident (when normalized to Fe(III) content), a fact which was also observed

DOI: 10.1021/acs.est.6b03015
Environ. Sci. Technol. 2016, 50, 11663−11671

Table 2. Kinetic Model and Rate Constants Used to Account for the Oxidation Behavior of Fe(II) in the Presence of O_2 and Dissolved Silicate[a]

no.	reaction	k (M^{-1} s^{-1})		
		pH 6	pH 6.5	pH 7
1	$Fe^{II} + O_2 \rightarrow Fe^{III} + O_2^-$	1.1×10^{-3}[b]	3.5×10^{-3}[b]	2.7×10^{-1}[c]
2	$Fe^{III} + Fe^{III} \rightarrow LEP + LEP$	1.0×10^{5}[d]	5.0×10^{5}[d]	1.0×10^{6}[d]
3[e]	$Fe^{II} + LEP \rightleftharpoons Fe^{II}$-LEP	5.0×10^{3}	2.4×10^{4}	4.3×10^{4}
4	Fe^{II}-LEP + $O_2 \rightarrow LEP + LEP_i$	4.96	80.2	88.7
5[e]	$Fe^{III} + Si \rightleftharpoons Fe^{III}$SiFHY	8.3×10^{4}	8.3×10^{4}	8.3×10^{4}
6	$Fe^{III}Si + Fe^{III}Si \rightarrow SiFHY + SiFHY$	2.5×10^{4}	3.5×10^{4}	1.0×10^{5}
7[e]	$Fe^{II} + SiF \rightleftharpoons Fe^{II}$-SiFHY	2.5×10^{2}	1.9×10^{3}	3.3×10^{3}
8	Fe^{II}-SiFHY + $O_2 \rightarrow SiFHY + SiFHY_i$	0.8	48.6	58.4

[a]Notes: LEP = lepidocrocite, LEP_i = internalized/nonreactive lepidocrocite SiFHY = silica ferrihydrite, $SiFHY_i$ = internalized/nonreactive silica ferrihydrite. [b]King.[3] [c]Pham and Waite.[4] [d]Values from Pham et al.[57] were used as a starting point and constrained to within 1 order of magnitude. [e]Values represent equilibrium constants (K) for reactions ($k_{formation}/k_{dissociation}$). All other values fitted from data collected in this study.

when dissolved silicate was added in Si:Fe molar ratios of 1 and 2 (SI Figure S6). A comparison of adsorbed Fe(II) in the absence (Figure 3) and presence (Figure S6) of silicate demonstrates that competitive sorption between Fe(II) and silicate across the measured pH range was minimal. However, a far greater proportion of Fe(II) was removed (or desorbed) from the silica-ferrihydrite reference solid upon extraction with $CaCl_2$, when compared to lepidocrocite (Figure 3; open symbols). This suggests that Fe(II) was sorbed to silica-ferrihydrite solids in a greater proportion of weaker, non-specific, outer-sphere sorption complexes, compared to lepidocrocite which contained a greater proportion of stronger, inner-sphere associations akin to that observed by Cismasu et al.[38] regarding Zn^{2+} sorption between ferrihydrite and silica-ferrihydrite.

Kinetic Modeling. A kinetic model was constructed using the reactions listed in Table 2. The model included the least number of reactions possible while still describing the Fe(II) oxidation data adequately. Further kinetic model information, assumptions and simplifications, can be found in the Supporting Information. Briefly, in the absence of silicate, Fe(II) oxidation was described by reactions 1−4, involving the homogeneous oxidation of Fe(II) (reaction #1), the precipitation of lepidocrocite (reaction #2), the faster adsorption of Fe(II) (inner-sphere only) to lepidocrocite and slower pH-dependent dissociative back reaction (equilibrium reaction #3, represented by K in eq 3), and the accelerated oxidation of the adsorbed Fe(II)-lepidocrocite species (reaction #4). A similar subset of reactions (reactions 1, and 5−8) were used to model the Fe(II) oxidation data in the presence of silicate, with the only difference being the inclusion of an Fe(III)-silicate complexation reaction.

The model outputs using the rate constants provided in Table 2 are represented by the solid lines in Figure 1. Additionally, sensitivity analyses were conducted to determine the importance of each reaction in Table 2 on changes to Fe(II) concentration (SI, Figure S7). The combined findings show that as pH decreased, in both the presence and absence of silicate, the relative importance of heterogeneous Fe(II) adsorption and oxidation increased in a manner similar to that observed by Jones et al.[5] under more acidic conditions. In particular, the sensitivity of the overall Fe(II) oxidation rate to inner-sphere Fe(II) adsorption (reaction #3) increased markedly with decreasing pH, as this mechanism becomes rate limiting. The calculated rate constants for heterogeneous Fe(II) oxidation at pH 6 for lepidocrocite are reasonably similar to those determined by Jones et al.[5] (1.89 M^{-1} s^{-1} at pH 5.5) and Tamura et al.[7] (1.12 M^{-1} s^{-1} at pH 6). The rate constant for Fe(II) oxidation in the presence of silica ferrihydrite is similar to that deduced by Jones et al.[5] at pH 5.5 (0.78 M^{-1} s^{-1}). However, our modeled rate constants increased substantially at pH 6.5 and 7 (Table 2). This pH-dependent deviation from previously modeled data is likely because Jones et al.[5] and Tamura et al.[7] measured Fe(II) oxidation rates in the presence of preformed Fe(III) oxides as opposed to the use of more reactive, in situ formed oxides in this study.

While the kinetic model provides a reasonable interpretation of the Fe(II) oxidation data, differences between the experimental results and modeling outcomes indicate that certain processes and effects have not been adequately captured. This may be due to intrinsic limitations in the simplified modeling of this complex system. For example, significant deviation between modeled data and empirical measurements was particularly evident at initial time points (Figure 1). In our view, these deviations were likely a consequence of the model being unable to describe key processes relating to initial Fe(III) polymerization and the heterogeneous nature of particle formation and aggregation, the kinetics of which are yet to be fully resolved.[47,48] Freshly formed Fe(III) polymers may have a limited capacity to adsorb Fe(II), and this could well be the reason for the observed Fe(II) oxidation "lag" at the beginning of each experiment. Also, the deviations observed toward the end of the experimental time period was likely due to the omission of any effects of aggregation and associated loss of solid phase reactivity in the simplified model.[47]

Linking Fe(II) Oxidation Products and Kinetics in the Presence of Silicate. The increasing addition of silicate (relative to Fe) alters both Fe(II) oxidation kinetics (i.e., retards oxidation) and changes the resulting Fe(III) solid phase to an increasing proportion of silica-ferrihydrite over lepidocrocite. Results from our adsorption studies show that absolute levels of Fe(II) sorption to lepidocrocite and silica-ferrihydrite (normalized to Fe(III) content) were similar, a finding contrary to previous observations regarding divalent metal uptake in the presence of Fe(III) oxides and oxyanions.[38] With silica-ferrihydrite having a vastly higher surface area (271.4 m^2/g) compared to lepidocrocite (61.6 m^2/g), one would expect different Fe(II) adsorption affinities though, as demonstrated by Choi et al.[49] in the case of lepidocrocite, surface area does not necessarily correlate with Fe(II) adsorption. Most likely the similar values between minerals

DOI: 10.1021/acs.est.6b03015
Environ. Sci. Technol. 2016, 50, 11663−11671

resulted from a combination of factors. First, Fe(II) uptake may be (disproportionally) kinetically limited across different Fe(III) oxides, as has been demonstrated previously.[50] The short Fe(II) adsorption period used in our experiments (10 min) in order to avoid mineral transformation may therefore have been responsible. It is also possible that our rigorous sample preparation involving multiple (and acidic) washing processes likely removed any surface precipitated Si, decreasing the capacity for silica-ferrihydrite to adsorb Fe(II), although solid Si loadings remained substantial (7.1 wt % or 27 mol %). Third, during silica-ferrihydrite mineral formation, reactive Fe(III) adsorption sites may simply be blocked by Si incorporation, preventing them from participating in surface binding, while still preserving high surface areas. And finally, the surface charge of the silica-ferrihydrite samples was between +10 and −10 mV across the pH range 6−7 (SI Figure S8), potentially limiting reactive surface site availability as a result of particle aggregation effects.

More critically though, extraction/desorption of Fe(II) with $CaCl_2$ (Figure 3) revealed that a greater proportion (~20 to 30% at any pH) of adsorbed Fe(II) was associated with weaker, outer-sphere complexes on the silica−ferrihydrite solid. As has previously been suggested by Cismasu et al.,[38] a greater electrostatic attraction between Fe(II), primarily present as Fe^{2+} (SI Figure S2), and the neutral to negatively charged silica-ferrihydrite, compared to the positively charged lepidocrocite surface (SI Figure S8) was likely responsible for this enhanced outer-sphere complexation. Furthermore, as indicated by Jones et al.,[5] Si will also likely have already bonded to reactive Fe(III) sites through oxygen coordination, limiting the opportunity for Fe(II)−Fe(III) inner-sphere complexation in silica−ferrihydrite.

A greater proportion of inner-sphere complexes/direct Fe(II) coordination with surface FeO_6 polyhedra associated with lepidocrocite will result in a greater electron density around the coordinated metal ion.[51] This therefore implies that the inner-sphere Fe(II) coordination with lepidocrocite will oxidize faster when compared to the electron-perturbed outer-sphere Fe(II) coordination associated with the silica-ferrihydrite which, as a result, will experience slower rates of electron transfer.[52] This mechanism provides a plausible explanation for the retarding effect of Si on heterogeneous Fe(II) oxidation kinetics.

Environmental Significance. This research provides an important advance in our understanding regarding rates of Fe(II) oxidation in the presence of silicate, with the findings applicable to a variety of systems involving fluctuating redox conditions. Although this is particularly relevant to the shallow trench-disposal site examined in this study, it is also applicable to other environments including similar LLRW sites,[53] sites Fe(0) or Fe(II) is used for the treatment of contaminated groundwaters (e.g., permeable reactive barriers, electrocoagulation)[54−56] and other sites with typically elevated silicate concentrations. Our research shows that dissolved silicate is a primary determinant of Fe(II) oxidation kinetics at the Little Forest study site with the presence of silicate significantly altering the rate of formation of one of the major sorbing phases. The importance of this finding is highlighted by the fact that water table fluctuations (along with associated mixing and transport) and Fe(II) oxidation kinetics operate on overlapping time scales. As Fe(III) oxides are capable of either retarding or mobilizing key radiochemical contaminants such as Pu,[29,31] information about their rates of formation in complex, multicomponent systems provides a valuable advance in our understanding of this phenomenon. These findings raise important questions regarding contaminant transport in high silicate environments, particularly with regard to the impact that more slowly forming but more reactive Fe(III) oxides such as silica-ferrihydrite exert on contaminant redox chemistry and the ensuing mobilization of these contaminants. Refs 55 and 56.

■ ASSOCIATED CONTENT

Supporting Information

The Supporting Information is available free of charge on the ACS Publications website at DOI: 10.1021/acs.est.6b03015.

Trench water ion composition, thermodynamic calculations, lepidocrocite and silica-ferrihydrite synthesis methods, Fe(II) oxidation kinetic data, FTIR and XAS data, Fe(II) sorption data, information on kinetic modeling is available in Supporting Information (PDF)

■ AUTHOR INFORMATION

Corresponding Author

*Phone: +61-2-9385-5060; e-mail: d.waite@unsw.edu.au.

Notes

The authors declare no competing financial interest.

■ ACKNOWLEDGMENTS

We gratefully acknowledge the following ANSTO staff: B. Rowling for support with field sampling; H. Wong, C. Vardanega and B. Rowling for inorganic analyses; and useful discussions with the remainder of the ANSTO IER team. The X-ray Absorption Spectroscopy research was undertaken on the XAS beamline at the Australian Synchrotron, Victoria, Australia.

■ REFERENCES

(1) Borch, T.; Kretzschmar, R.; Kappler, A.; Cappellen, P. V.; Ginder-Vogel, M.; Voegelin, A.; Campbell, K. Biogeochemical redox processes and their impact on contaminant dynamics. *Environ. Sci. Technol.* **2010**, *44* (1), 15−23.

(2) Sung, W.; Morgan, J. J. Kinetics and product of ferrous iron oxygenation in aqueous systems. *Environ. Sci. Technol.* **1980**, *14* (5), 561−568.

(3) King, D. W. Role of carbonate speciation on the oxidation rate of Fe(II) in aquatic systems. *Environ. Sci. Technol.* **1998**, *32* (19), 2997−3003.

(4) Pham, A. N.; Waite, T. D. Oxygenation of Fe(II) in natural waters revisited: Kinetic modeling approaches, rate constant estimation and the importance of various reaction pathways. *Geochim. Cosmochim. Acta* **2008**, *72* (15), 3616−3630.

(5) Jones, A. M.; Griffin, P. J.; Collins, R. N.; Waite, T. D. Ferrous iron oxidation under acidic conditions − The effect of ferric oxide surfaces. *Geochim. Cosmochim. Acta* **2014**, *145* (0), 1−12.

(6) Tamura, H.; Goto, K.; Nagayama, M. The effect of ferric hydroxide on the oxygenation of ferrous ions in neutral solutions. *Corros. Sci.* **1976**, *16* (4), 197−207.

(7) Tamura, H.; Kawamura, S.; Hagayama, M. Acceleration of the oxidation of Fe^{2+} ions by Fe(III)-oxyhydroxides. *Corros. Sci.* **1980**, *20* (8−9), 963−971.

(8) Jones, A. M.; Griffin, P. J.; Waite, T. D. Ferrous iron oxidation by molecular oxygen under acidic conditions: The effect of citrate, EDTA and fulvic acid. *Geochim. Cosmochim. Acta* **2015**, *160*, 117−131.

(9) Rose, A. L.; Waite, T. D. Kinetic model for Fe(II) oxidation in seawater in the absence and presence of natural organic matter. *Environ. Sci. Technol.* **2002**, *36* (3), 433−444.

(10) Schenk, J. E.; Weber, W. J. Chemical interactions of dissolved silica with iron (II) and (III). *J. Am. Water Works Assoc.* **1968**, *60* (2), 199−212.

DOI: 10.1021/acs.est.6b03015
Environ. Sci. Technol. 2016, 50, 11663−11671

(11) Tamura, H.; Goto, K.; Nagayama, M. Effect of anions on the oxygenation of ferrous ion in neutral solutions. *J. Inorg. Nucl. Chem.* **1976**, *38* (1), 113−117.
(12) Wolthoorn, A.; Temminghoff, E. J. M.; Weng, L.; Van Riemsdijk, W. H. Colloid formation in groundwater: Effect of phosphate, manganese, silicate and dissolved organic matter on the dynamic heterogeneous oxidation of ferrous iron. *Appl. Geochem.* **2004**, *19* (4), 611−622.
(13) Jones, A. M.; Collins, R. N.; Rose, J.; Waite, T. D. The effect of silica and natural organic matter on the Fe(II)-catalysed transformation and reactivity of Fe(III) minerals. *Geochim. Cosmochim. Acta* **2009**, *73* (15), 4409−4422.
(14) Pokrovski, G. S.; Schott, J.; Farges, F.; Hazemann, J. L. Iron (III)-silica interactions in aqueous solution: Insights from X-ray absorption fine structure spectroscopy. *Geochim. Cosmochim. Acta* **2003**, *67* (19), 3559−3573.
(15) Schwertmann, U.; Thalmann, H. The influence of [Fe(II)], [Si], and pH on the formation of lepidocrocite and ferrihydrite during oxidation of aqueous $FeCl_2$ solutions. *Clay Miner.* **1976**, *11* (3), 189−200.
(16) Doelsch, E.; Rose, J.; Masion, A.; Bottero, J. Y.; Nahon, D.; Bertsch, P. M. Speciation and crystal chemistry of iron(III) chloride hydrolyzed in the presence of SiO4 ligands. 1. An Fe K-edge EXAFS study. *Langmuir* **2000**, *16* (10), 4726−4731.
(17) Kaegi, R.; Voegelin, A.; Folini, D.; Hug, S. J. Effect of phosphate, silicate, and Ca on the morphology, structure and elemental composition of Fe(III)-precipitates formed in aerated Fe(II) and As(III) containing water. *Geochim. Cosmochim. Acta* **2010**, *74* (20), 5798−5816.
(18) Mayer, T. D.; Jarrell, W. M. Formation and stability of iron(II) oxidation products under natural concentrations of dissolved silica. *Water Res.* **1996**, *30* (5), 1208−1214.
(19) Senn, A. C.; Kaegi, R.; Hug, S. J.; Hering, J. G.; Mangold, S.; Voegelin, A. Composition and structure of Fe(III)-precipitates formed by Fe(II) oxidation in water at near-neutral pH: Interdependent effects of phosphate, silicate and Ca. *Geochim. Cosmochim. Acta* **2015**, *162*, 220−246.
(20) Swedlund, P. J.; Webster, J. G. Adsorption and polymerisation of silicic acid on ferrihydrite, and its effect on arsenic adsorption. *Water Res.* **1999**, *33* (16), 3413−3422.
(21) Voegelin, A.; Kaegi, R.; Frommer, J.; Vantelon, D.; Hug, S. J. Effect of phosphate, silicate, and Ca on Fe(III)-precipitates formed in aerated Fe(II)- and As(III)-containing water studied by X-ray absorption spectroscopy. *Geochim. Cosmochim. Acta* **2010**, *74* (1), 164−186.
(22) Cismasu, A. C.; Michel, F. M.; Tcaciuc, A. P.; Brown, G. E. Properties of impurity-bearing ferrihydrite III. Effects of Si on the structure of 2-line ferrihydrite. *Geochim. Cosmochim. Acta* **2014**, *133*, 168−185.
(23) Van Genuchten, C. M.; Peña, J.; Amrose, S. E.; Gadgil, A. J. Structure of Fe(III) precipitates generated by the electrolytic dissolution of Fe(0) in the presence of groundwater ions. *Geochim. Cosmochim. Acta* **2014**, *127*, 285−304.
(24) Green, R.; Waite, T. D.; Melville, M. D.; Macdonald, B. C. T. Characteristics of the acidity in acid sulfate soil drainage waters, McLeods Creek, northeastern NSW, Australia. *Environ. Chem.* **2006**, *3* (3), 225−232.
(25) Cundy, A. B.; Hopkinson, L.; Whitby, R. L. D. Use of iron-based technologies in contaminated land and groundwater remediation: A review. *Sci. Total Environ.* **2008**, *400* (1−3), 42−51.
(26) Nordstrom, D. K.; Blowes, D. W.; Ptacek, C. J. Hydrogeochemistry and microbiology of mine drainage: An update. *Appl. Geochem.* **2015**, *57*, 3−16.
(27) Ikeda-Ohno, A.; Harrison, J. J.; Thiruvoth, S.; Wilsher, K.; Wong, H. K. Y.; Johansen, M. P.; Waite, T. D.; Payne, T. E. Solution speciation of plutonium and americium at an Australian legacy radioactive waste disposal site. *Environ. Sci. Technol.* **2014**, *48* (17), 10045−10053.
(28) Payne, T. E.; Harrison, J. J.; Hughes, C. E.; Johansen, M. P.; Thiruvoth, S.; Wilsher, K. L.; Cendón, D. I.; Hankin, S. I.; Rowling, B.; Zawadzki, A. Trench 'bathtubbing' and surface plutonium contamination at a legacy radioactive waste site. *Environ. Sci. Technol.* **2013**, *47* (23), 13284−13293.
(29) Kersting, A. B. Plutonium transport in the environment. *Inorg. Chem.* **2013**, *52* (7), 3533−3546.
(30) Kersting, A. B.; Efurd, D. W.; Finnegan, D. L.; Rokop, D. J.; Smith, D. K.; Thompson, J. L. Migration of plutonium in ground water at the Nevada Test Site. *Nature* **1999**, *397* (6714), 56−59.
(31) Novikov, A. P.; Kalmykov, S. N.; Utsunomiya, S.; Ewing, R. C.; Horreard, F.; Merkulov, A.; Clark, S. B.; Tkachev, V. V.; Myasoedov, B. F. Colloid transport of plutonium in the far-field of the Mayak Production Association, Russia. *Science* **2006**, *314* (5799), 638−641.
(32) Cendón, D. I.; Hughes, C. E.; Harrison, J. J.; Hankin, S. I.; Johansen, M. P.; Payne, T. E.; Wong, H.; Rowling, B.; Vine, M.; Wilsher, K.; Guinea, A.; Thiruvoth, S. Identification of sources and processes in a low-level radioactive waste site adjacent to landfills: groundwater hydrogeochemistry and isotopes. *Aust. J. Earth Sci.* **2015**, *62* (1), 123−141.
(33) Hughes, C. E.; Cendón, D. I.; Harrison, J. J.; Hankin, S. I.; Johansen, M. P.; Payne, T. E.; Vine, M.; Collins, R. N.; Hoffmann, E. L.; Loosz, T. Movement of a tritium plume in shallow groundwater at a legacy low-level radioactive waste disposal site in eastern Australia. *J. Environ. Radioact.* **2011**, *102* (10), 943−952.
(34) Payne, T. E. *Background report on the Little Forest Burial Ground legacy waste site (ANSTO E-780)*; Institute for Environmental Research, Australian Nuclear Science and Technology Organisation, 2012; p 25.
(35) Cornell, R. M.; Schwertmann, U. *The Iron Oxides: Structure, Properties, Reactions, Occurences and Uses*; Wiley-VCH: Weinheim, 2003.
(36) Kandegedara, A.; Rorabacher, D. B. Noncomplexing tertiary amines as 'better' buffers covering the range of pH 3−11. Temperature dependence of their acid dissociation constants. *Anal. Chem.* **1999**, *71* (15), 3140−3144.
(37) APHA. *Standard Methods for the Examination of Water and Wastewater*, 20th ed.; American Public Health Association, American Water Works Association, Water Environment Federation: Baltimore, 1998.
(38) Cismasu, A. C.; Levard, C.; Michel, F. M.; Brown, G. E., Jr Properties of impurity-bearing ferrihydrite II: Insights into the surface structure and composition of pure, Al- and Si-bearing ferrihydrite from Zn(II) sorption experiments and Zn K-edge X-ray absorption spectroscopy. *Geochim. Cosmochim. Acta* **2013**, *119*, 46−60.
(39) Ravel, B.; Newville, M. ATHENA, ARTEMIS, HEPHAESTUS: data analysis for X-ray absorption spectroscopy using IFEFFIT. *J. Synchrotron Radiat.* **2005**, *12*, 537−541.
(40) Johnson, K. A.; Simpson, Z. B.; Blom, T. Global Kinetic Explorer: A new computer program for dynamic simulation and fitting of kinetic data. *Anal. Biochem.* **2009**, *387* (1), 20−29.
(41) Ianni, J. C., Kintecus Windows version 5.20. 2014. www.kintecus.com.
(42) Santana-Casiano, J. M.; González-Dávila, M.; Millero, F. J. The oxidation of Fe(II) in NaCl-HCO_3^- and seawater solutions in the presence of phthalate and salicylate ions: A kinetic model. *Mar. Chem.* **2004**, *85* (1−2), 27−40.
(43) Lewis, D. G.; Farmer, V. C. Infrared absorption of surface hydroxyl groups and lattice vibrations in lepidocrocite (g-FeOOH) and boehmite (g-AlOOH). *Clay Miner.* **1986**, *21* (1), 93−100.
(44) Carlson, L.; Schwertmann, U. Natural ferrihydrites in surface deposits from Finland and their association with silica. *Geochim. Cosmochim. Acta* **1981**, *45* (3), 421−425 427−429.
(45) Swedlund, P. J.; Sivaloganathan, S.; Miskelly, G. M.; Waterhouse, G. I. N. Assessing the role of silicate polymerization on metal oxyhydroxide surfaces using X-ray photoelectron spectroscopy. *Chem. Geol.* **2011**, *285* (1−4), 62−69.
(46) Châtellier, X.; West, M. M.; Rose, J.; Fortin, D.; Leppard, G. G.; Ferris, F. G. Characterization of iron-oxides formed by oxidation of

DOI: 10.1021/acs.est.6b03015
Environ. Sci. Technol. 2016, 50, 11663−11671

ferrous ions in the presence of various bacterial species and inorganic ligands. *Geomicrobiol. J.* **2004**, *21* (2), 99−112.
(47) Bligh, M. W.; Waite, T. D. Formation, aggregation and reactivity of amorphous ferric oxyhydroxides on dissociation of Fe(III)-organic complexes in dilute aqueous suspensions. *Geochim. Cosmochim. Acta* **2010**, *74* (20), 5746−5762.
(48) Rose, A. L.; Bligh, M. W.; Collins, R. N.; Waite, T. D. Resolving early stages of homogeneous iron(III) oxyhydroxide formation from iron(III) nitrate solutions at pH 3 using time-resolved SAXS. *Langmuir* **2014**, *30* (12), 3548−3556.
(49) Choi, S.; Hong, S.; Ahn, K.; Baumann, E. R. Adsorption of ferrous iron on the lepidocrocite surface. *Environ. Technol.* **2001**, *22* (3), 355−365.
(50) Joen, B. H.; Dempsey, B. A.; Burgos, W. D. Kinetics and mechanisms for reactions of Fe(II) with iron(III) oxides. *Environ. Sci. Technol.* **2003**, *37* (15), 3309−3315.
(51) Stumm, W.; Morgan, M. D. *Aquatic Chemistry: Chemical Equilibria and Rates in Natural Waters*; 3rd ed.; Wiley: New York, 1996.
(52) Jones, A. M.; Kinsela, A. S.; Collins, R. N.; Waite, T. D. The reduction of 4-chloronitrobenzene by Fe(II)-Fe(III) oxide systems - correlations with reduction potential and inhibition by silicate. *J. Hazard. Mater.* **2016**, *320*, 143−149.
(53) Stewart, B. D.; Cismasu, A. C.; Williams, K. H.; Peyton, B. M.; Nico, P. S. Reactivity of uranium and ferrous iron with natural iron oxyhydroxides. *Environ. Sci. Technol.* **2015**, *49* (17), 10357−10365.
(54) Blowes, D. W.; Ptacek, C. J.; Benner, S. G.; McRae, C. W. T.; Bennett, T. A.; Puls, R. W. Treatment of inorganic contaminants using permeable reactive barriers. *J. Contam. Hydrol.* **2000**, *45* (1−2), 123−137.
(55) Kanel, S. R.; Manning, B.; Charlet, L.; Choi, H. Removal of arsenic(III) from groundwater by nanoscale zero-valent iron. *Environ. Sci. Technol.* **2005**, *39* (5), 1291−1298.
(56) Van Genuchten, C. M.; Addy, S. E. A.; Peña, J.; Gadgil, A. J. Removing arsenic from synthetic groundwater with iron electrocoagulation: An Fe and As K-edge EXAFS study. *Environ. Sci. Technol.* **2012**, *46* (2), 986−994.
(57) Pham, A. N.; Rose, A. L.; Feitz, A. J.; Waite, T. D. Kinetics of Fe(III) precipitation in aqueous solutions at pH 6.0−9.5 and 25°C. *Geochim. Cosmochim. Acta* **2006**, *70* (3), 640−650.

DOI: 10.1021/acs.est.6b03015
Environ. Sci. Technol. 2016, 50, 11663−11671